CMS Physics Analysis Summary

Contact: cms-pag-conveners-top@cern.ch 2016/08/04

Measurement of particle level differential $\mathrm{t\bar{t}}$ cross sections in the dilepton channel at $\sqrt{s} = 13\,\mathrm{TeV}$

The CMS Collaboration

Abstract

Normalised differential cross sections for top quark pair production are measured in the dilepton (e^+e^-, $\mu^+\mu^-$, and $\mu^\mp e^\pm$) decay channel in proton-proton collisions at a center-of-mass energy of 13 TeV. The measurements are performed with data corresponding to an integrated luminosity of 2.2 fb^{-1} collected in 2015 using the CMS detector at the LHC. The cross section is measured differentially as a function of the kinematic properties of the leptons, b jets, top quarks, and top quark pairs at particle level. The results are compared to several models of perturbative QCD and found to be in agreement with the standard model predictions.

1 Introduction

The top quark is the heaviest elementary particle known, and its corresponding expected strong coupling to the Higgs boson suggests it could play an important role in explaining the mechanism of electroweak symmetry breaking. Many new physics models predict new particles leading to final states similar to that of top quark-antiquark pairs ($t\bar{t}$). The precise measurement of the $t\bar{t}$ differential cross section can lead to a better understanding of background contributions [1], and provides a good test of perturbative QCD calculations.

The normalised $t\bar{t}$ differential cross section is measured in the dilepton channel as a function of the $t\bar{t}$ system, top quark, and daughter lepton and b jet kinematic properties such as transverse momentum, rapidity, invariant mass and azimuthal decorrelation [2].

We present the measurement at particle level with final state objects defined in a theoretically safe and unambiguous way. The particle level measurements are expected to reduce the dependence on the theoretical model, so variables are mainly corrected for detector effects. The measurement is performed in the visible phase space to avoid large extrapolations into regions that are not experimentally accessible.

2 Data and simulated samples

We use $\sqrt{s}$ = 13 TeV proton-proton (pp) collision data, corresponding to an integrated luminosity of 2.2 fb^{-1} collected in 2015 with the CMS detector at the CERN LHC [3]. At least two leptons (electrons or muons) are required at trigger level, a lepton with $p_{\text{T}} > 17\,\text{GeV}$ and a second lepton with $p_{\text{T}} > 12\,\text{GeV}$ for an electron or $p_{\text{T}} > 8\,\text{GeV}$ for a muon.

Monte Carlo (MC) simulated event samples are used to model the $t\bar{t}$ signal and the background processes. We use the POWHEG (v2) [4] generator to model the nominal $t\bar{t}$ signal at the next-to-leading order (NLO) in QCD, assuming a top quark mass of 172.5 GeV. The data are also compared to predictions of MG5_aMC@NLO (v2.2.2) [5], which includes the NLO matrix elements (ME) for up to two partons in addition to the $t\bar{t}$ pair, and MADGRAPH, which includes the ME for up to three partons at LO. The parton distribution functions (PDF) used in the MG5_aMC@NLO sample is `NNPDF30_lo_as_0130`, while all other samples used `NNPDF30_NLO_as_0118` [6]. The parton shower (PS) is modelled using PYTHIA 8 (v8.205) [7] in which the tune CUETP8M1 [8] is used to model the underlying event. The matching to the ME partons is done using the `FXFX` [9] algorithm for the NLO generators and `MLM` [10] for the LO generators. The signal samples are normalised to the next-to-next-to-leading order (NNLO) calculated cross section [11].

For the Drell-Yan + jets process decaying into dilepton pairs ($Z/\gamma^* \to l^+l^-$), MG5_aMC@NLO is used with the dilepton invariant mass at generator level satisfying $M(l^+l^-) > 10\,\text{GeV}$. The W boson + jets samples are generated with MG5_aMC@NLO and normalised using the NNLO calculated cross sections [12]. The single top quark production in the tW-channel is simulated with the POWHEG generator based on the five flavour scheme, and normalised using the NLO calculated cross sections [13]. The diboson samples (WW, WZ and ZZ) are generated using PYTHIA 8 and normalised using the NNLO calculated cross sections for the WW sample [14] and NLO for the WZ and ZZ samples.

Additional pp collisions (pileup) are simulated with PYTHIA 8 and superimposed on the hard scattering events using a pileup multiplicity distribution that reflects the luminosity profile of the analysed data. The detector response to the final state particles is simulated using GEANT4 [15], and the events are reconstructed and analysed with the same software used to

process the data.

3 Object and event selection

The dilepton final state of the $t\bar{t}$ decay consists of two leptons (electrons or muons), at least two jets, and missing transverse momentum from two neutrinos. The Particle Flow (PF) algorithm [16, 17] is used to reconstruct objects in the event, using global information from the CMS detector.

Muons are reconstructed by a global fit to the track using information from the tracker and muon systems. The muons are required to have $p_{\mathrm{T}} > 20\,\mathrm{GeV}$ and $|\eta| < 2.4$. Quality requirements are imposed on the number of hits and on the association of the muon track to the primary vertex of the event [18].

To reduce the secondary leptons from multijet background, isolation criteria are applied. For muons, the isolation requirement accounts for the contribution from additional particles from pileup:

$$I_{\mathrm{rel}}(\mu) = \frac{\sum p_T^{\mathrm{CH}} + \max\left(0, \sum p_T^{\mathrm{NH}} + \sum p_T^{\gamma} - \frac{1}{2} \times \sum p_T^{\text{PU-CH}}\right)}{p_T^{\mu}} < 0.15,$$

where the superscripts CH, NH, γ, and PU-CH denote charged hadrons from the primary vertex, neutral hadrons, photons, and charged hadrons from the pileup vertices, respectively. The momentum is summed inside a radius of $\Delta R = \sqrt{\Delta\phi^2 + \Delta\eta^2} < 0.4$.

Electrons are reconstructed using the Gaussian Sum Filter algorithm [19] for the inner tracker track and matched to an electromagnetic calorimeter (ECAL) cluster. The electrons are required to have $p_{\mathrm{T}} > 20\,\mathrm{GeV}$ and $|\eta| < 2.4$. We use the identification criteria designed to give an average efficiency of around 80% [20]. We reject electrons traversing through the barrel-endcap transition region of the ECAL, corresponding to a calorimeter cluster position of $1.4442 < |\eta| < 1.566$. The electron selection also includes an isolation criterion, depending on the pseudorapidity of the calorimeter cluster.

Mismodelling of the lepton selection and trigger efficiencies in simulation are accounted for by applying scale factors derived using data-driven techniques [21, 22].

Jets are reconstructed using PF candidates as inputs to the anti-k_{T} jet clustering algorithm [23, 24], with the distance parameter set to 0.4 [25]. The momenta of jets are corrected to account for effects from pileup and non-uniformity and non-linearity of the detector [26]. For the data, residual energy corrections are also applied to account for residual mismodelling of the MC response. We select jets with $p_{\mathrm{T}} > 30\,\mathrm{GeV}$ and $|\eta| < 2.4$ which pass loose identification criteria designed to reject noise in the calorimeters.

Jets from B hadron decay are identified by the Combined Secondary Vertex (CSV) b tagging algorithm. This algorithm uses several input variables including the information from the secondary vertices. We select jets using a loose working point corresponding to a rate of misidentifying a light flavour jet as a b quark jet of 10% [27, 28]. The b tagging efficiency in the simulation is corrected to be consistent with the data.

The missing transverse energy ($E_{\mathrm{T}}^{\mathrm{miss}}$) is calculated from the imbalance of the transverse momentum of all PF candidates in the event following energy corrections [17, 29]. Since neutrinos in the $t\bar{t}$ dilepton channel are reconstructed from the missing transverse momentum of the

event, $E_{\mathrm{T}}^{\mathrm{miss}}$ is an important variable in reconstructing the top quark kinematics.

We require events with exactly two opposite-charge leptons with $M(l^+l^-) > 20\,\mathrm{GeV}$, and at least two jets, at least one of which has to be identified as a b quark jet. In addition, for the same-flavour lepton channels (ee and $\mu\mu$), additional selection criteria are applied designed to reject events from Drell-Yan production: $E_{\mathrm{T}}^{\mathrm{miss}} > 40\,\mathrm{GeV}$ and $|M(l^+l^-) - M_{\mathrm{Z}}| > 15\,\mathrm{GeV}$, where $M_{\mathrm{Z}} = 91\,\mathrm{GeV}$.

4 Signal definition at particle level

We define the particle level top quark following the generator level prescriptions used in Ref. [30]. This approach avoids differences in the top quark definition due to possible differences in the decay history of different generators, and leads to results that are expected to be independent of the generator implementation and tuning.

The top quarks are reconstructed starting from the final state particles in $\mathrm{t\bar{t}}$ events at generator level as summarised in Tab.1. To avoid the ambiguity from additional leptons at generator level, a distinction is made between prompt particles and particles from hadron decays. Leptons are dressed using the anti-k_{T} clustering algorithm with a distance parameter of 0.1 to account for final state radiated photons. The clustering is applied on prompt electrons, muons and photons. Events with leptons from prompt τ decay are treated as background. Leptons are required to satisfy the same acceptance requirements as imposed on the reconstructed objects described in Sec. 3, $p_{\mathrm{T}} > 20\,\mathrm{GeV}$ and $|\eta| < 2.4$.

The generator level jets are clustered with the anti-k_{T} algorithm with a distance parameter of 0.4 applied on all final state particles except neutrinos and the particles already included in the dressed leptons. Jets are required to have $p_{\mathrm{T}} > 30\,\mathrm{GeV}$ and $|\eta| < 2.4$ to be consistent with the reconstructed object selection. To identify the flavour of the jet we use the ghost B hadron technique [31], where B hadrons are included in the jet clustering after scaling down their momentum to be negligible. A jet is identified as a b quark jet if it contains any B hadrons among its constituents.

Table 1: Summary of object definitions at the particle level

Object	Definition	Selection criteria
Prompt neutrino	neutrinos not from hadron decay	none
Dressed lepton	anti-k_{T} jet with a distance parameter of 0.1 using electrons, muons and photons not from hadron decay	$p_{\mathrm{T}} > 20\,\mathrm{GeV}$, $\|\eta\| < 2.4$
b quark jet	anti-k_{T} jet with a distance parameter of 0.4 using all particles and ghost B hadrons not including any neutrinos nor particles used in dressed leptons	$p_{\mathrm{T}} > 30\,\mathrm{GeV}$, $\|\eta\| < 2.4$ with ghost B hadrons

Pseudo-W bosons are reconstructed by combining a dressed lepton and a prompt neutrino. A pair of pseudo-W bosons is chosen among the possible combinations to minimise the scalar sum of invariant mass differences with respect to the W boson mass of 80.4 GeV [32]. Similarly, the pseudo-top quarks are defined by combining a pseudo-W boson and a b quark jet, with an invariant mass requirement of 172.5 GeV. The visible phase space is defined to have a pair of pseudo-top quarks, constructed from prompt neutrinos, dressed leptons and b quark jets. Events that are not in the visible phase space are considered as background.

5 Systematic uncertainties

The systematic uncertainties in the lepton identification and isolation efficiencies are determined by varying the measured scale factors by their total uncertainties. For the trigger selection, the systematic uncertainty is calculated 'antagonistically' depending on the $|\eta|$ combinations of the first and second legs: $\pm 1\sigma$ for barrel-barrel, $\mp 1\sigma$ for endcap-endcap, and $\pm 0.5\sigma$ for barrel-endcap and endcap-barrel.

The pileup distribution used in the simulation is based on a central value of the total inelastic pp cross section of 69 mb, which is varied by $\pm 5\%$ to determine the associated systematic uncertainty. Uncertainties in the jet energy scale (JES) and jet energy resolution (JER) are determined on a per-jet basis using a tag and probe method, and propagated to the event level quantities [33].

For the theoretical uncertainties, we investigate the effect of the choice of PDFs, factorisation and renormalisation scales (μ_F and μ_R) at ME and PS level, different top quark masses, and hadronisation and generator modelling. The eigenvector sets of the `NNPDF30_NLO_as_0118` parametrisation are used to calculate the PDF uncertainty [6]. We measure 100 individual uncertainties and take the root-mean-square as the PDF uncertainty following the PDF4LHC recommendation [34]. The MC modelling uncertainties are estimated by comparing the POWHEG and MG5_aMC@NLO generators. The uncertainty from the choice of μ_F and μ_R is estimated by varying the scales independently by a factor of two up and down (but not in opposite directions), and taking the envelope of the differences with respect to the nominal parameter choice. The scale uncertainty in the parton shower is assessed by changing μ_F and μ_R together up and down by a factor of two. We evaluate the top quark mass uncertainty by taking the maximum deviation between the nominal sample with a top quark mass of 172.5 GeV and two different top quark mass samples of 171.5 GeV and 173.5 GeV. The uncertainty from hadronisation and parton shower modelling is estimated by comparing the results obtained from POWHEG samples interfaced to PYTHIA 8 and HERWIG++.

The uncertainty in the background normalisation is estimated based on a 30% variation [35] of the background yields.

Typical systematic uncertainties for some of the kinematic variables that will be introduced in Sec. 6 are presented in Tab. 2, which lists the median value for each systematic uncertainty source in each kinematic distribution. The dominant sources for systematic uncertainty are due to the modelling, hadronisation and background estimation.

6 Normalised differential cross section

We measure the normalised differential $\mathrm{t\bar{t}}$ cross section $(1/\sigma)(\mathrm{d}\sigma/\mathrm{d}X)$ as a function of several different kinematic variables X. The variables include the transverse momenta of leptons (p_{T}^{l}), jets (p_{T}^{j}), top quarks ($p_{\mathrm{T}}^{\mathrm{t}}$), and the $\mathrm{t\bar{t}}$ system ($p_{\mathrm{T}}^{\mathrm{t\bar{t}}}$), the rapidities of the top quarks (y^{t}) and the $\mathrm{t\bar{t}}$ system ($y^{\mathrm{t\bar{t}}}$), and the invariant mass of the $\mathrm{t\bar{t}}$ system ($M^{\mathrm{t\bar{t}}}$). In addition, we measure the differential cross section as a function of the azimuthal angle between the top quarks $\Delta\phi^{\mathrm{t\bar{t}}}$ to investigate the azimuthal decorrelation of top quarks, which is particularly sensitive to the presence of new physics. The measurements are compared to several standard model predictions.

In the $\mathrm{t\bar{t}}$ dilepton channel, the reconstruction of the neutrino and antineutrino is crucial in determining the top quark kinematics. Using an analytical approach [36, 37], the six unknown neutrino degrees of freedom are constrained by the two measured components of the miss-

Table 2: Median systematic uncertainties in the normalised differential cross section for three representative kinematic variables. The maximum over all measured variables is given in the last column.

Systematic uncertainty	Median of p_T^t [%]	Median of $p_T^{t\bar{t}}$ [%]	Median of $\Delta\phi^{t\bar{t}}$ [%]	Maximum of median [%]
Trigger	1	1	1	1
Pileup	1	1	1	1
Lepton SF	1	1	1	1
JES	1	1	1	2
JER	2	1	1	2
b jet SF	1	2	1	2
Background	3	3	4	6
μ_F and μ_R	1	4	5	5
MC modelling	3	7	12	12
Top quark mass	1	4	5	5
Hadronisation	6	4	2	6
PDF	1	1	1	2

ing transverse momentum and the assumed invariant masses of both W boson and top quark systems.

The top quark reconstruction method is very similar to that used in the recent CMS measurement of the differential $t\bar{t}$ cross section at parton level [22], but is performed at particle level. To allow for the finite resolution of the measured objects the $t\bar{t}$ system is reconstructed for 100 random variations within their simulated resolution functions, and the W boson mass is also allowed to vary over its Breit-Wigner distribution. In each trial there are up to eight solutions [36], and we select the solution with the minimum invariant mass of the $t\bar{t}$ system. For each trial, a weight is calculated using the expected invariant mass distribution of lepton and b quark jet pairs (M_{lb}) at particle level. The reconstructed neutrino momentum is taken from the weighted average over the trials. The final solution of the $t\bar{t}$ system is the solution with the maximum weight. The efficiency of the kinematic reconstruction is approximately 90%.

The kinematics of the leptons, b quark jets, top quarks, and $t\bar{t}$ system are taken from the selected final solution. Figure 1 shows the distributions of p_T^l, p_T^j, p_T^t, and y^t, while Figure 2 shows the distributions of $p_T^{t\bar{t}}$, $y^{t\bar{t}}$, $M^{t\bar{t}}$, and $\Delta\phi^{t\bar{t}}$. In the top panel of each figure, the data points are compared to the sum of the expected contributions. The bottom panel shows the ratio of the data to the expectations.

The width of each bin in the distributions is chosen to control event migration between reconstruction- and generator-level bins due to detector efficiencies and resolutions. We compute the purity (stability), defined as the number of events both generated and correctly reconstructed in a certain bin divided by the total number of events in the reconstruction-level (generator-level) bin, and the bin width is chosen to give purity and stability of about 50%.

In order to measure the top quark kinematic distribution in the visible phase space, we first remove the contributions from backgrounds. Non-$t\bar{t}$ backgrounds are subtracted from the measured distributions. The $t\bar{t}$ backgrounds (including events from outside the visible phase space and events not from the dilepton channel, and denoted $t\bar{t}$-others) are then removed as a proportion of the total $t\bar{t}$ contribution by applying a correction factor k as defined in Eq. 1:

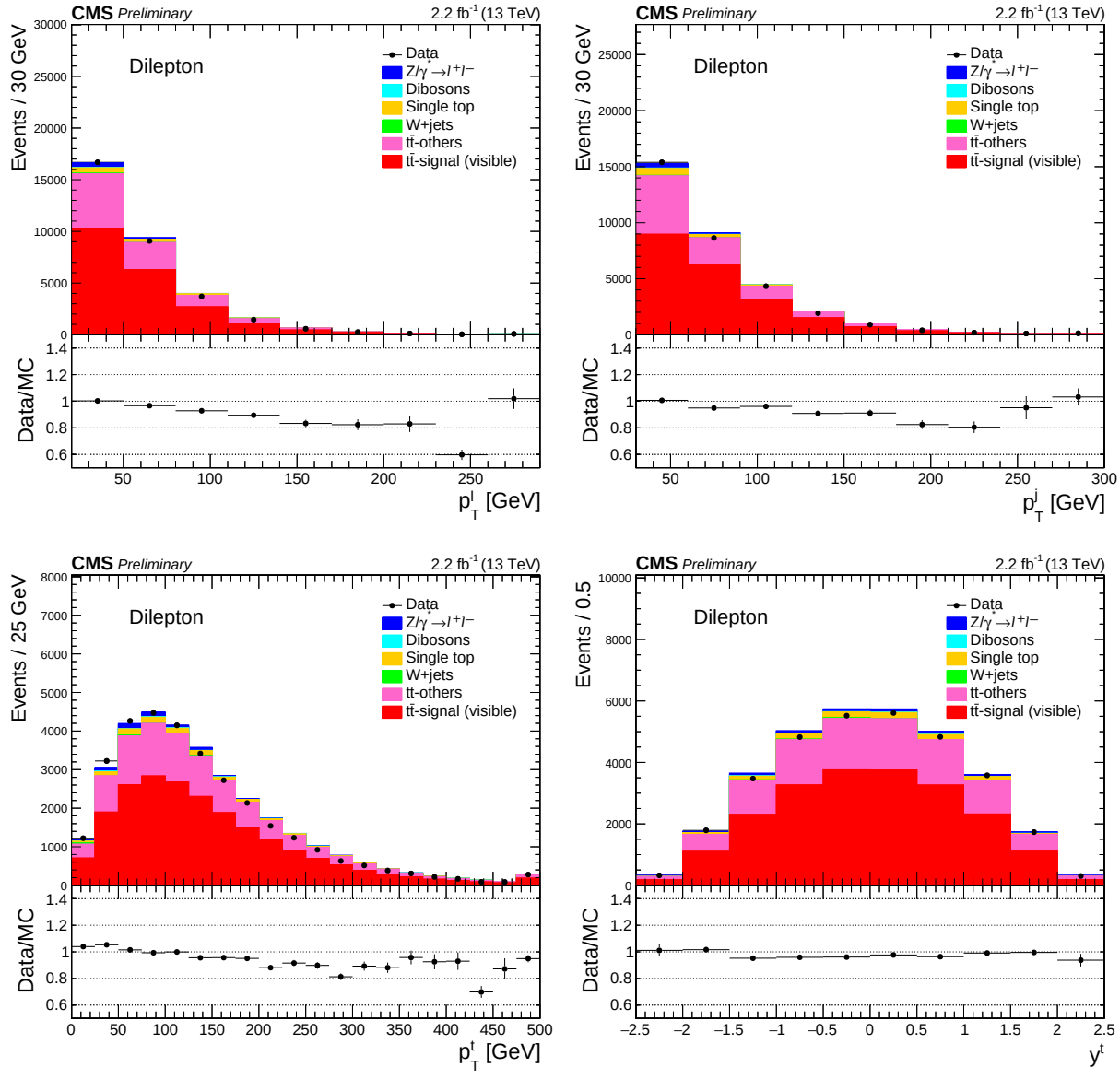

Figure 1: Reconstructed p_T^l, p_T^j, p_T^t, and y^t distributions. All corrections described in the text are applied to the simulation.

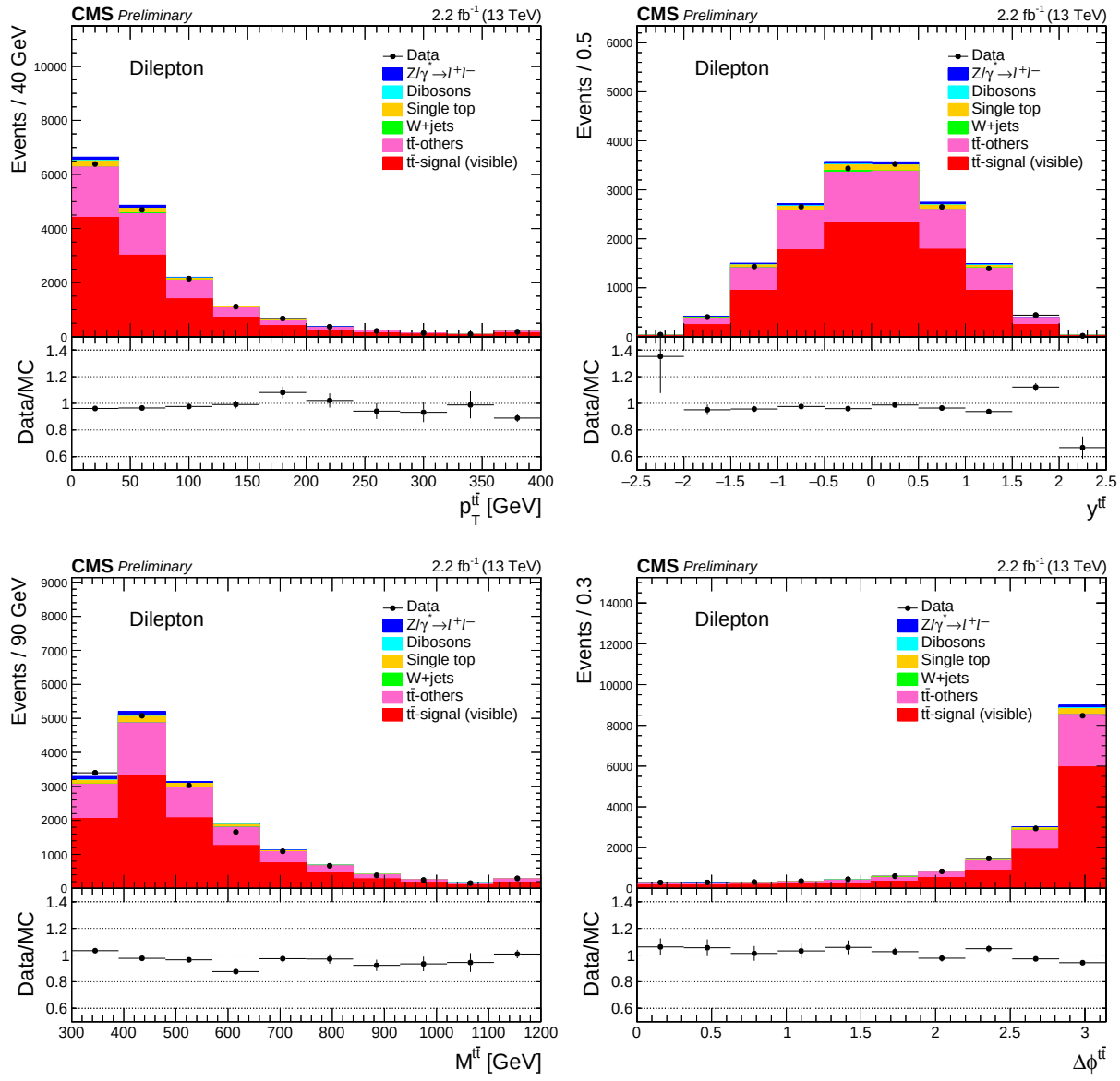

Figure 2: Reconstructed $p_T^{t\bar{t}}$, $y^{t\bar{t}}$, $M^{t\bar{t}}$, and $\Delta\phi^{t\bar{t}}$ distributions. All corrections described in the text are applied to the simulation.

$$k = \frac{N_{\text{data}} - N_{\text{MC,bkg}}}{N_{\text{MC,t}\bar{\text{t}}-\text{signal}} + N_{\text{MC,t}\bar{\text{t}}-\text{others}}}\,, \qquad (1)$$
$$N_{\text{data,t}\bar{\text{t}}-\text{signal}} = N_{\text{data}} - N_{\text{MC,bkg}} - kN_{\text{MC,t}\bar{\text{t}}-\text{others}}\,.$$

Here, $N_{\text{MC,bkg}}$ is the estimate for the non-$\text{t}\bar{\text{t}}$ background, $N_{\text{MC,t}\bar{\text{t}}-\text{signal}}$ is the MC predicted $\text{t}\bar{\text{t}}$ signal yield, and $N_{\text{MC,t}\bar{\text{t}}-\text{others}}$ is the remaining MC $\text{t}\bar{\text{t}}$ yield. We find $k \sim 0.95$, and the $\text{t}\bar{\text{t}}$ signal yield, $N_{\text{data,t}\bar{\text{t}}-\text{signal}}$, is then extracted in each bin as shown in the lower part of Eq. 1.

Detector resolution and reconstruction efficiency effects are corrected by using an unfolding procedure. The method relies on a response matrix which maps the expected relation between the true and reconstructed variables. D'Agostini's method is employed to perform the unfolding [38–40]. The effective regularisation strength of the iterative D'Agostini unfolding is controlled by the number of iterations. A small number of iterations can bias to the measurement towards the simulated prediction, while with a large number of iterations the result converges to that of matrix inversion. The number of iterations is optimised for each distribution, using simulation to find the minimum number of iterations that keeps the bias to a negligible level [41].

Figures 3 and 4 show the normalised differential $\text{t}\bar{\text{t}}$ cross section as a function of p_T^l, p_T^j, p_T^t, y^t, $p_T^{\text{t}\bar{\text{t}}}$, $y^{\text{t}\bar{\text{t}}}$, $M^{\text{t}\bar{\text{t}}}$, and $\Delta\phi^{\text{t}\bar{\text{t}}}$ at particle level in the visible phase space. The measured data are compared to different standard model predictions from POWHEG +PYTHIA 8, MG5_aMC@NLO +PYTHIA 8 [FXFX], MG5_aMC@NLO +PYTHIA 8 [MLM], and POWHEG +HERWIG++. The main experimental systematic uncertainties are related to the uncertainty in the modelling in simulation of the lepton trigger, isolation and identification efficiencies, pileup, JES, JER, and b jet tagging efficiency.

In general, the POWHEG +HERWIG++ prediction better describes the data than the predictions interfaced with PYTHIA 8, with the exception of the $M^{\text{t}\bar{\text{t}}}$ distribution. The lepton p_T spectrum in data tends to be softer than the MC predictions for $p_T > 100$ GeV. A similar trend is also observed in the top quark p_T spectrum, although it is in agreement with predictions within the uncertainties. The measurements are generally found to be in agreement with the standard model predictions.

7 Summary

The normalised differential cross section for top quark pair production is measured in the dilepton decay channel in pp collisions at $\sqrt{s} = 13$ TeV with data corresponding to an integrated luminosity of 2.2 fb^{-1}. The differential cross section is measured as a function of p_T^l, p_T^j, p_T^t, y^t, $p_T^{\text{t}\bar{\text{t}}}$, $y^{\text{t}\bar{\text{t}}}$, $M^{\text{t}\bar{\text{t}}}$, and $\Delta\phi^{\text{t}\bar{\text{t}}}$ at particle level in the visible phase space. The measurements are compared to the predictions from POWHEG +PYTHIA 8, MG5_aMC@NLO +PYTHIA 8 [FXFX], MG5_aMC@NLO +PYTHIA 8 [MLM], and POWHEG +HERWIG++, and are found to be in agreement with the standard model.

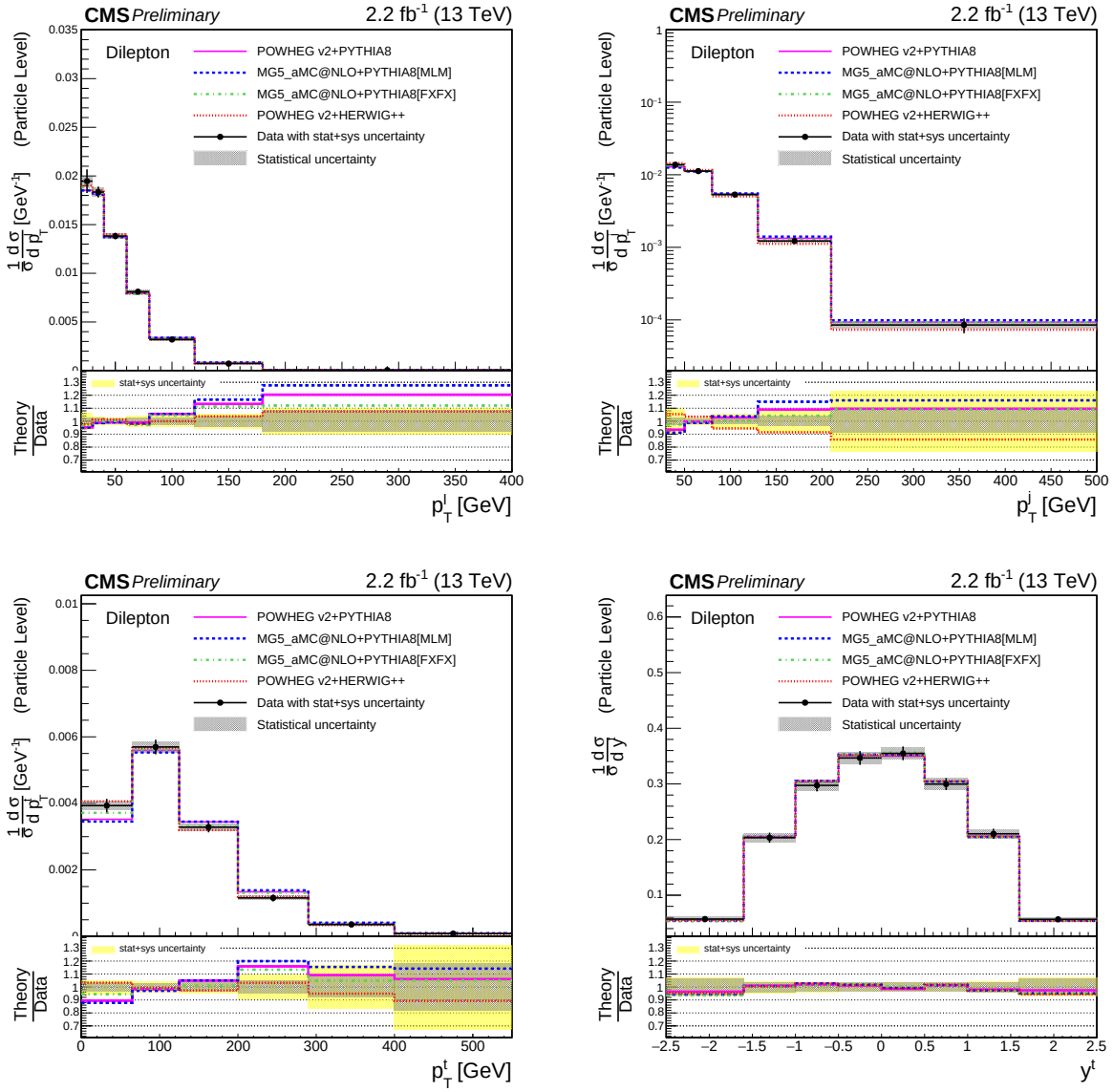

Figure 3: Normalised differential cross section as a function of lepton, jet, and top quark p_{T} and top quark rapidity, measured at particle level in the visible phase space and combining the distributions for top quarks and antiquarks. The error bars on the data points indicate the total (combined statistical and systematic) uncertainties, while the dark shaded band shows the statistical uncertainty. The measurements are compared to predictions from POWHEG +PYTHIA 8, MG5_aMC@NLO +PYTHIA 8 [FXFX], MG5_aMC@NLO +PYTHIA 8 [MLM], and POWHEG +HERWIG++.

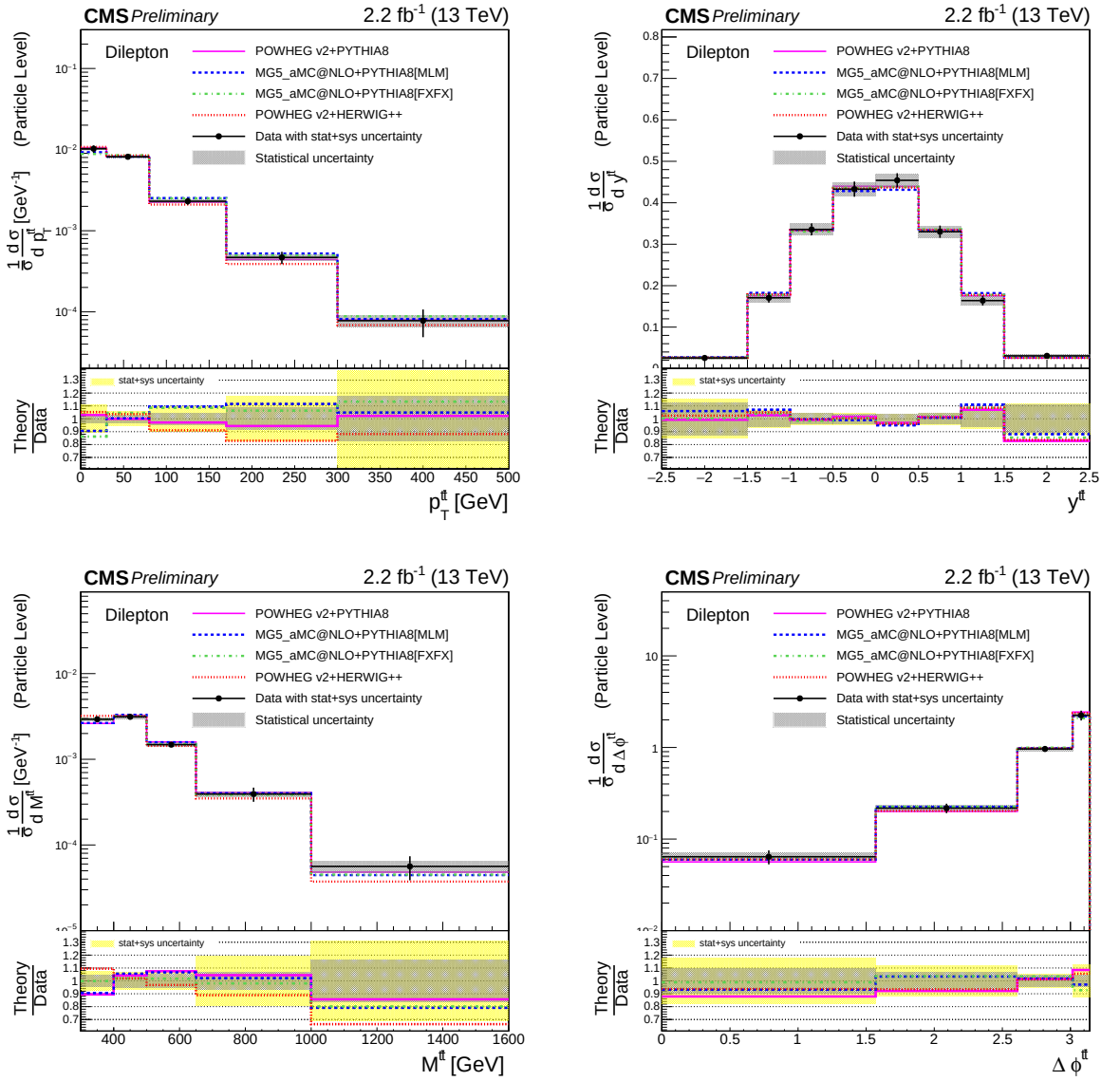

Figure 4: Normalised differential cross section as a function of $p_T^{t\bar{t}}$, $y^{t\bar{t}}$, $M^{t\bar{t}}$, and $\Delta\phi^{t\bar{t}}$ for the top quarks or antiquarks, measured at particle level in the visible phase space. The error bars on the data points indicate the total (combined statistical and systematic) uncertainties, while the dark shaded band shows the statistical uncertainty. The measurements are compared to predictions from POWHEG +PYTHIA 8, MG5_aMC@NLO +PYTHIA 8 [FXFX], MG5_aMC@NLO +PYTHIA 8 [MLM], and POWHEG +HERWIG++.

References

[1] A. Denner, S. Dittmaier, S. Kallweit, and S. Pozzorini, "NLO QCD corrections to off-shell $t\bar{t}$ production at hadron colliders", *PoS* **LL2012** (2012) 015, arXiv:1208.4053.

[2] S. Choi and H. S. Lee, "Azimuthal decorrelation in $t\bar{t}$ production at hadron colliders", *Phys. Rev. D* **87** (2013), no. 3, 034012, doi:10.1103/PhysRevD.87.034012, arXiv:1207.1484.

[3] CMS Collaboration, "The CMS experiment at the CERN LHC", *Journal of Instrumentation* **3** (2008), no. 08, S08004, doi:10.1088/1748-0221/3/08/S08004.

[4] S. Alioli, P. Nason, C. Oleari, and E. Re, "A general framework for implementing NLO calculations in shower Monte Carlo programs: the POWHEG BOX", *JHEP* **06** (2010) 043, doi:10.1007/JHEP06(2010)043, arXiv:1002.2581.

[5] J. Alwall et al., "The automated computation of tree-level and next-to-leading order differential cross sections, and their matching to parton shower simulations", *JHEP* **07** (2014) 079, doi:10.1007/JHEP07(2014)079, arXiv:1405.0301.

[6] NNPDF Collaboration, "Parton distributions for the LHC Run II", *JHEP* **04** (2015) 040, doi:10.1007/JHEP04(2015)040, arXiv:1410.8849.

[7] T. Sjostrand, S. Mrenna, and P. Z. Skands, "A Brief Introduction to PYTHIA 8.1", *Comput. Phys. Commun.* **178** (2008) 852–867, doi:10.1016/j.cpc.2008.01.036, arXiv:0710.3820.

[8] P. Skands, S. Carrazza, and J. Rojo, "Tuning PYTHIA 8.1: the Monash 2013 Tune", *Eur. Phys. J. C* **74** (2014) 3024, doi:10.1140/epjc/s10052-014-3024-y, arXiv:1404.5630.

[9] R. Frederix and S. Frixione, "Merging meets matching in MC@NLO", *JHEP* **12** (2012) 061, doi:10.1007/JHEP12(2012)061, arXiv:1209.6215.

[10] S. Hoeche et al., "Matching parton showers and matrix elements", in *HERA and the LHC: A Workshop on the implications of HERA for LHC physics: Proceedings Part A*. 2006. arXiv:hep-ph/0602031.

[11] M. Czakon and A. Mitov, "Top++: A Program for the Calculation of the Top-Pair Cross-Section at Hadron Colliders", *Comput. Phys. Commun.* **185** (2014) 2930, doi:10.1016/j.cpc.2014.06.021, arXiv:1112.5675.

[12] Y. Li and F. Petriello, "Combining QCD and electroweak corrections to dilepton production in FEWZ", *Phys. Rev. D* **86** (2012) 094034, doi:10.1103/PhysRevD.86.094034, arXiv:1208.5967.

[13] N. Kidonakis, "NNLL threshold resummation for top-pair and single-top production", *Phys. Part. Nucl.* **45** (2014), no. 4, 714–722, doi:10.1134/S1063779614040091, arXiv:1210.7813.

[14] T. Gehrmann et al., "W^+W^- Production at Hadron Colliders in Next to Next to Leading Order QCD", *Phys. Rev. Lett.* **113** (Nov, 2014) 212001, doi:10.1103/PhysRevLett.113.212001.

[15] J. Allison et al., "Geant4 developments and applications", *IEEE Trans. Nucl. Sci.* **53** (2006) 270, doi:10.1109/TNS.2006.869826.

[16] CMS Collaboration, "Commissioning of the Particle-flow Event Reconstruction with the first LHC collisions recorded in the CMS detector", CMS Physics Analysis Summary CMS-PAS-PFT-10-001, 2010.

[17] CMS Collaboration, "Particle-flow event reconstruction in CMS and performance for jets, taus, and $E_{\mathrm{T}}^{\mathrm{miss}}$", CMS Physics Analysis Summary CMS-PAS-PFT-09-001, 2009.

[18] CMS Collaboration, "Performance of CMS muon reconstruction in pp collision events at $\sqrt{s} = 7$ TeV", *Journal of Instrumentation* **7** (October, 2012) P10002, doi:10.1088/1748-0221/7/10/P10002, arXiv:1206.4071.

[19] W. Adam, R. Fruhwirth, A. Strandlie, and T. Todor, "Reconstruction of Electrons with the Gaussian-Sum Filter in the CMS Tracker at the LHC", CMS Note CMS-NOTE-2005-001, 2005.

[20] CMS Collaboration, "Electron and Photon performance using data collected by CMS at $\sqrt{s}$ = 13 TeV and 25ns", CMS Detector Performance Summaries CMS-DP-2015-067, 2015.

[21] CMS Collaboration, "Muon Reconstruction and Identification Improvements for Run-2 and First Results with 2015 Run Data", CMS Detector Performance Summaries CMS-DP-2015-015, 2015.

[22] CMS Collaboration, "Measurement of the differential cross section for $\mathrm{t\bar{t}}$ production in the dilepton final state at $\sqrt{s} = 13$ TeV", CMS Physics Analysis Summary CMS-PAS-TOP-16-011, 2016.

[23] M. Cacciari, G. P. Salam, and G. Soyez, "FastJet User Manual", *Eur. Phys. J.* **C72** (2012) 1896, doi:10.1140/epjc/s10052-012-1896-2, arXiv:1111.6097.

[24] M. Cacciari, G. P. Salam, and G. Soyez, "The anti-k_T jet clustering algorithm", *JHEP* **04** (2008) 063, doi:10.1088/1126-6708/2008/04/063, arXiv:0802.1189.

[25] CMS Collaboration, "Jet energy scale and resolution in the CMS experiment in pp collisions at 8 TeV", CMS Physics Analysis Summary CERN-PH-EP-2015-305, 2016.

[26] CMS Collaboration, "Jet energy scale and resolution performances with 13TeV data", CMS Detector Performance Summaries CMS-DP-2016-020, 2016.

[27] CMS Collaboration, "Identification of b quark jets at the CMS Experiment in the LHC Run 2", CMS Physics Analysis Summary CMS-PAS-BTV-15-001, 2016.

[28] CMS Collaboration, "b-Jet Identification in the CMS Experiment", CMS Physics Analysis Summary CMS-PAS-BTV-11-004, 2012.

[29] CMS Collaboration, "MET performance in 8 TeV data", CMS Physics Analysis Summary CMS-PAS-JME-12-002, 2012.

[30] CMS Collaboration, "Comparisons of Theory Predictions for the $\mathrm{t\bar{t}}$ Process with Data from pp Collisions at $\sqrt{s}$= 8 TeV", CMS Physics Analysis Summary CMS-PAS-TOP-15-011, 2015.

[31] M. Cacciari and G. P. Salam, "Pileup subtraction using jet areas", *Phys. Lett. B* **659** (2008), no. 12, 119 – 126, doi:http://dx.doi.org/10.1016/j.physletb.2007.09.077.

[32] Particle Data Group Collaboration, "Review of Particle Physics", *Chin. Phys. C* **38** (2014) 090001, doi:10.1088/1674-1137/38/9/090001.

[33] CMS Collaboration, "Determination of jet energy calibration and transverse momentum resolution in CMS", *Journal of Instrumentation* **6** (2011), no. 11, P11002, doi:10.1088/1748-0221/6/11/P11002.

[34] J. Butterworth et al., "PDF4LHC recommendations for LHC Run II", *J. Phys. G* **43** (2016) 023001, doi:10.1088/0954-3899/43/2/023001, arXiv:1510.03865.

[35] CMS Collaboration, "Measurement of the top quark pair production cross section in proton-proton collisions at $\sqrt{(s)} = 13$ TeV", *Phys. Rev. Lett.* **116** (2016), no. 5, 052002, doi:10.1103/PhysRevLett.116.052002, arXiv:1510.05302.

[36] L. Sonnenschein, "Analytical solution of $t\bar{t}$ dilepton equations", *Phys. Rev. D* **73** (2006) 054015, doi:10.1103/PhysRevD.78.079902, 10.1103/PhysRevD.73.054015, arXiv:hep-ph/0603011. [Erratum: Phys. Rev.D78,079902(2008)].

[37] R. H. Dalitz and G. R. Goldstein, "Analysis of top-antitop production and dilepton decay events and the top quark mass", *Phys. Lett. B* **287** (1992) 225–230, doi:10.1016/0370-2693(92)91904-N.

[38] T. Adye, "Unfolding algorithms and tests using RooUnfold", Technical Report arXiv:1105.1160, May, 2011.

[39] G.D'Agostini., "A multidimensional unfolding method based on Bayes", *Nuclear Instruments and Methods in Physics Research A* **362:487-498** (February 1995).

[40] G. D'Agostini, "Improved iterative Bayesian unfolding", ArXiv, October, 2010. arXiv:1010.0632.

[41] CMS Collaboration, "Measurement of the inclusive and differential tt production cross sections in lepton + jets final states at 13 TeV", CMS Physics Analysis Summary CMS-PAS-TOP-16-008, 2016.